Relation between shape of liquid-gas interface and evolution of buoyantly unstable three-dimensional chemical fronts

L. Šebestíková*

Institute of Hydrodynamics, Academy of Sciences of the Czech Republic, Pod Patankou 30/5, 16612 Praha 6, Czech Republic

(Received 5 December 2012; revised manuscript received 8 August 2013; published 27 September 2013)

Buoyantly unstable 3D chemical fronts were seen traveling through an iodate-arsenous acid reaction solution. The experiments were performed in channel reactors with rectangular cross sections, where the top of the reaction solution was in contact with air. A concave or convex meniscus was pinned to reactor lateral walls. Influence of the meniscus shape on front development was investigated. For the concave meniscus, an asymptotic shape of fronts holding negative curvature was observed. On the other hand, fronts propagating in the solution with the convex meniscus kept only positive curvature. Those fronts were also a bit faster than fronts propagating in the solution with the concave meniscus. A relation between the meniscus shape, flow distribution, velocity, and shape is discussed.

DOI: 10.1103/PhysRevE.88.033023 PACS number(s): 47.20.Bp, 82.40.Ck

I. INTRODUCTION

Traveling chemical waves have been intensively studied over the last several decades [1–11]. Two types of chemical waves, pulses and fronts, can be distinguished. Pulses can be generated in the reaction mixture repeatedly. On the other hand, a chemical front can pass through the reaction mixture just once. However, both types of waves are invading the reaction mixture because of coupling of an autocatalytic reaction and diffusion. In liquid media, natural convection can also be involved. Natural convection can be generated by a chemical reaction, which causes changes of surface tension, density, or viscosity. Both solutal and thermal effects could contribute to those processes. Although the natural convection is connected to the chemical reaction, the convection is independent of the type of chemical wave. The chemical waves play other roles. For miscible solutions, the wave separates reactants and products from each other without formation of interfacial tension. Therefore, the wave serves as a special kind of physical interface. The wave is also the site where gradients of physical properties are located. The interaction of chemical waves and the natural convection has been studied for several chemical systems, among others the Belousov-Zhabotinsky (BZ) reaction and the iodate-arsenous acid (IAA) reaction. In the BZ reaction system, primarily effects of Marangoni convection on traveling pulses were studied [9,12–16]. In the IAA reaction system, the influence of density-driven convection on fronts was investigated [2,3,7,8,11,17–22].

The IAA reaction can be written in two consequent steps [Eq. (1) and Eq. (2)] [2], the linear combination of which determines the net reaction stoichiometry and composition of product solutions:

$$IO_3^- + 5I^- + 6H^+ \rightarrow 3I_2 + 3H_2O, \tag{1}$$

$$H_3AsO_3 + I_2 + H_2O \rightarrow 2I^- + H_3AsO_4 + 2H^+. \tag{2}$$

Depending on the stoichiometric ratio R,

$$R = \frac{[H_3AsO_3]}{[IO_3^-]}, \tag{3}$$

where $[\cdot]$ denotes concentration of the reactants iodate (IO_3^-) and arsenous acid (H_3AsO_3), three different regimes with respect to product composition are possible: (1) stoichiometric excess of arsenous acid (i.e., $R > 3.0$), where iodide (I^-) is the product and iodine (I_2) is an intermediate; (2) stoichiometric excess of iodate ($R < 2.5$), where iodine is the product and iodide is an intermediate; and (3) when none of the components is in stoichiometric excess ($2.5 \leqslant R \leqslant 3.0$), arsenous acid and iodate are fully consumed, and both iodide and iodine are the products.

The buoyancy effects on the IAA reaction system were studied experimentally in two- (2D) [3,17,22] and three-dimensional (3D) [7] arrangements and theoretically in 2D arrangements [20,21,23]. Pojman *et al*. [3,17] determined that density of the reactants is due to the thermal and solutal effects higher than the density of products. Therefore, the descending fronts are stable, whereas the ascending and vertical fronts are buoyantly unstable. In all studies the vertical fronts were tilted in lateral views, and the tilted fronts were accompanied by single convection roll [3,7,17,18,20]. Although the fronts propagated with constant velocities, the velocities were increasing with solution depth [7,20–22].

This article reports the influence of a naturally formed meniscus on IAA reaction front development. The fronts propagated through a horizontal layer of the IAA reaction solution placed in a channel reactor. The top of the reactor was open to air. Liquid was pinned to reactor lateral walls so a concave or a convex meniscus was formed. A relation between the meniscus shape, convection, and front evolution is presented and discussed.

II. EXPERIMENTS

The experiments were carried out with the IAA reaction solution containing a stoichiometric excess of arsenous acid. The net reaction stoichiometry then reads

$$IO_3^- + 3H_3AsO_3 \rightarrow I^- + 3H_3AsO_4. \tag{4}$$

*lenka@n2.cz

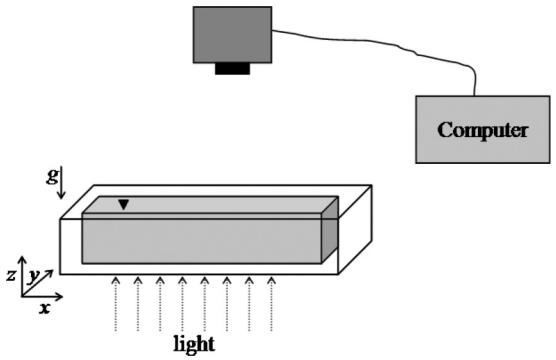

FIG. 1. Experimental arrangement. The experiments were performed in a plexiglass channel reactor illuminated from below. Top views were directly recorded by the camera.

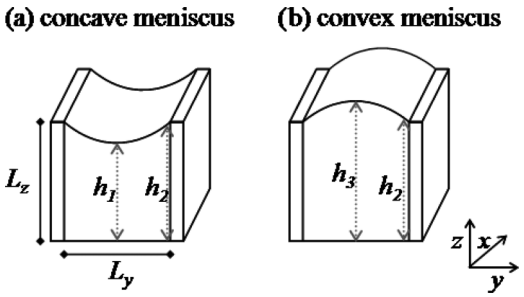

FIG. 2. Liquid layer shape. (a) The concave meniscus; (b) the convex meniscus. h_1 and h_3 were measured for $y = 1/2\ L_y$. $h_2 = L_z$ was measured at the reactor lateral walls for both experimental conditions. The maximal and minimal layer depth was located as follows: $h_{\min} = h_1$ and $h_{\max} = h_2$ for the concave meniscus and $h_{\min} = h_2$ and $h_{\max} = h_3$ for the convex meniscus.

The experiments were performed with chemicals provided by Merck with the quality of analytical standards. The reaction solutions were prepared from stock solutions and their temperature held constant at $21 \pm 1\,^{\circ}$C. The fresh reaction mixtures contained 0.016 M $NaAsO_2$, 0.016 M H_2SO_4, and 0.005 M $NaIO_3$, which gives the ratio $R = 3.2$. In order to visualize the reaction progress, the fresh starch solution (0.06% w/v) was added to the reaction mixture. The starch solution forms a dark blue complex with iodine, the intermediate of the reaction. Therefore, for $R > 3$, solutions containing either reactants or final products of the IAA reaction are colorless. The dark blue is seen only where the reaction is running.

Concentrations of reaction species were chosen the same as those used in the IAA experiments performed in channel reactors [7], in Hele-Shaw cells [19], in capillary tubes [3,17], and in Petri dishes filled with gel media [5]. This gives us the opportunity to compare our current experimental results with previously published studies. For a reaction solution containing 0.005 M $NaIO_3$, Pojman *et al.* [17] determined the total density difference ($\Delta\rho = -1.6\times 10^{-4}$ g/cm^3). Our measured pH values ($p\mathrm{H}_{\mathrm{reactants}} = 2.05 \pm 0.04$, $p\mathrm{H}_{\mathrm{products}} = 1.88 \pm 0.04$) are in agreement with both Šebestiková *et al.* [7] ($p\mathrm{H}_{\mathrm{reactants}} = 2.11 \pm 0.01$, $p\mathrm{H}_{\mathrm{products}} = 1.92 \pm 0.01$) and Forštová *et al.* [5] ($p\mathrm{H}_{\mathrm{reactants}} = 2.14 \pm 0.04$, $p\mathrm{H}_{\mathrm{products}} = 1.92 \pm 0.06$).

The experimental setup consists of a channel reactor, cold light source, and video camera; see Fig. 1. Channel reactors with rectangular cross sections were made from transparent plexiglass. Inner sizes of the used channel reactors were length L_x 90 mm, width L_y 15 mm, and reactor height L_z 2, 3, and 4 mm, respectively. The cold desk light source illuminated experiments from below. Top views of the channel reactor were recorded by using the computer-connected video camera.

Freshly prepared reaction solutions were injected into the reactor. The volume of the solution was chosen so either a concave or convex meniscus was formed. The meniscus was pinned to the reactor edges for all performed experiments; see Fig. 2. The reached reaction solution depth depended on L_z and the type of the meniscus. The difference between the maximal ($h_{\max}$) and minimal ($h_{\min}$) solution height was 0.5 mm. For a concave meniscus, $h_{\max}$ was at lateral walls, and $h_{\min}$ was at $L_y = 1/2$. For a convex meniscus, the situation was the opposite, $h_{\max}$ was at $L_y = 1/2$, and $h_{\min}$ was at lateral walls. Particular heights of the reaction solution are summarized in Table I, where $h_1 = h_{\min}$ and $h_2 = h_{\max}$ for concave meniscus, and $h_2 = h_{\min}$ and $h_3 = h_{\max}$ for convex meniscus.

Immediately after filling, the chemical front was initiated chemically by using a pipet tip filled with 20 μl of the product solution. The tip was carefully and slowly moved towards the reaction solution, where the tip got in contact with the interface. The short and very gentle touch did not induce any visible movement of the interface. Diffusion flux of products from the filled tip into the fresh reactant solution was sufficient to immediately start the reaction at the contact location without any need to actively inject any volume of the product solution. The fronts were initiated on the left side of the reactor so they invaded the reaction solution from left to right. We should note that the same results would be obtained for fronts propagating from right to left if the channel reactor is placed horizontally. After the front initiation, the reactor was covered by a transparent plexiglass box in order to prevent air movement caused by an air conditioning device. However, an air layer, which remained between the reaction solution and the cover, was at least 10 mm thick. The progress of experiments was recorded from the moment when the reactor was filled with the reaction solution. The temperature in the reactor and in its environment was kept constant at $21 \pm 1\,^{\circ}$C by the laboratory air conditioning device.

Measurements of surface tension of reactants, products, and iodine-water solutions were performed with a Tensiometer K11 MK2 (Krüss GmbH, Hamburg, Germany). Surface tension was measured at $21\,^{\circ}$C by both Wilhelmy plate methods and De Noüy ring methods. Fresh reaction solutions were prepared as described above. Iodine-water solutions were prepared by dissolution of solid iodine in distilled water

TABLE I. The height of the reactor wall (L_z) and the corresponding liquid layer depth (h_i). The layer depth was measured at both reactor walls and at $y = 1/2L_y$; for details see Fig. 2.

L_z (mm)	h_1 (mm)	h_2 (mm)	h_3 (mm)
2	1.5	2	2.5
3	2.5	3	3.5
4	3.5	4	4.5

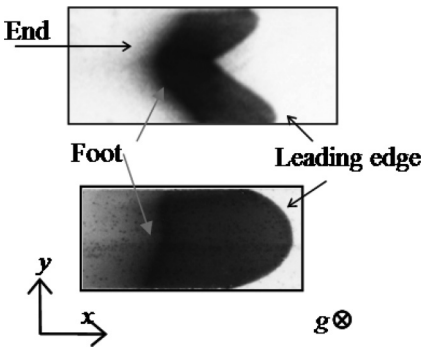

FIG. 3. Definition of front parts seen on top views.

($c_{I_2} = 0.4$ mM). For the reaction solutions, surface tension was measured both before the reaction had started and when the reaction was completely finished. For all measured solutions, surface tension was determined to be 71 ± 1 mN/m, which corresponds to water containing inorganic ions.

III. RESULTS

The fronts were 3D objects developing in time. After the initiation, the fronts propagated in all directions. This initial period ended when the fronts approached the rector bottom and the reactor lateral walls. The fronts then traveled along the reactor from its left end to its right end. Fronts shown on top views look like a dark spot; see Fig. 3. The right border of the spot delineates the front head, which is located at the liquid-gas interface. This is the front leading edge. The opposite border is called the front end. Finally, the front foot, which is the front head located at the reactor bottom, is seen as a darker curve inside the gray spot. In lateral views, tilted fronts were observed.

Figure 4 shows the shape of fronts in dependency on the layer depth and the meniscus shape. All images show fronts when their leading edges were approximately at $1/2\ L_x$ except one image, where the leading edge was approximately at $3/4\ L_x$. Under the concave meniscus condition, leading edges, foots, and ends had a V-like shape with negative curvature. Under the convex meniscus condition, the front leading edges and front foots had a parabolic shape with positive curvature. The front ends were seen as parabolic only for $L_z < 4$ mm. For $L_z = 4$ mm, the very fuzzy front end made determination of the shape problematic. Under both experimental conditions, distances between the leading edge and the foot and distances between the leading edge and the end were increasing with L_z.

Distance between the leading edge and the foot defines mixing length (W_{bulk}) of liquid motion passing through the

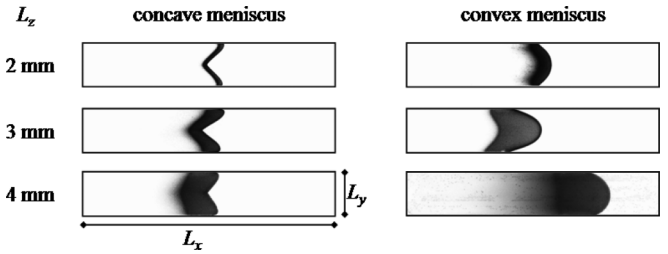

FIG. 4. Dependence of the front shape on the solution layer depth and the meniscus shape. $L_y = 15$ mm, $L_x = 90$ mm.

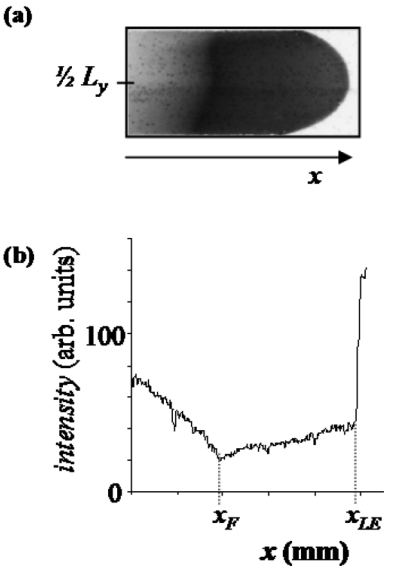

FIG. 5. Determination of the front leading edge x_{LE} and the front foot x_F. (a) An original image; (b) an intensity profile obtained from the original image along the x coordinate at $y = 1/2\ L_y$. The obtained x_{LE} and x_F were then included in Eq. (5), from which the mixing length W_{bulk} was calculated.

liquid layer. Determination of the mixing length W_{bulk} was done as follows:

$$W_{\text{bulk}} = \sqrt{h^2 + (x_{LE} - x_F)^2}, \tag{5}$$

where h is the solution depth, x_{LE} is the position of the leading edge, and x_F is the position of the foot. x_{LE} and x_F were determined by the following procedure. At first, for chosen position y, to which corresponded particular h, a color intensity profile was obtained from an original image; see Fig. 5. On the intensity profiles, the clear white and the clear black are represented by values 255 and 0, respectively. Under this condition, the darker color seen as the lower number of the color intensity was obtained. In Fig. 5(b), color intensity profiles consist of three characteristic parts. Reading from right to left, a very fast drop is replaced by a slow decrease, which is followed by a faster increase. The place where the intensity falls, is the position of the leading edge x_{LE}. The place where the slow decrease is changed into the increase is the position of the foot x_F. When values of x_{LE} and x_F are known, a corresponding mixing length W_{bulk} can be calculated.

In order to examine time development of the particular W_{bulk}, space-time plots were constructed from the original images. For a chosen position y, 1 pixel thick windows were cut along the x coordinate. The size of such window was then 1 pixel times 90 mm. Those windows were placed in chronological order. The time period between two consequent windows was 1 s. Figures 6(a) and 6(b) shows space-time plots of fronts propagating along the reactor under both convex and concave meniscus conditions, respectively. Except for the beginning and the end of the experiment, the front traces look like tilted stripes of constant thickness. The right border of the stripe shows the position of the leading edge. The left border traces the foot. Traces of the leading edge and the foot are parallel. Therefore, mixing length W_{bulk}, which is given by the distance between leading edge and foot, was constant for

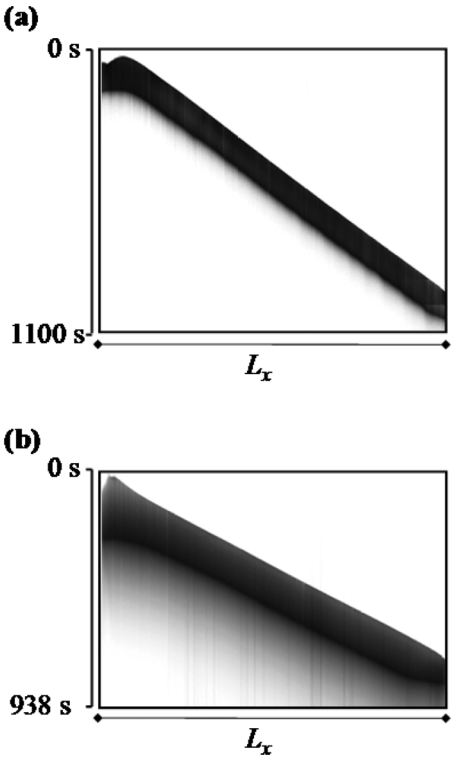

FIG. 6. Space-time plots. (a) The concave meniscus; (b) the convex meniscus. $L_x = 90$ mm, $L_z = 4$ mm.

chosen liquid layer depth h. This result allowed us to evaluate W_{bulk} from one particular image. Images, where the leading edge was approximately at position $x = 1/2\ L_x$, were chosen for W_{bulk} evaluation.

Dependence of the mixing length W_{bulk} on h is shown in Fig. 7. Under both concave and convex meniscus conditions, W_{bulk} is increasing with h. However, higher values of W_{bulk} are seen for $h > 2.5$ mm under the convex meniscus condition. Those values were obtained for measurements performed at $y = 1/2\ L_y$, where the liquid depth h is equal to $h_{\max}$.

Figure 8 shows development of the front leading edge for both concave and convex meniscus conditions. During the

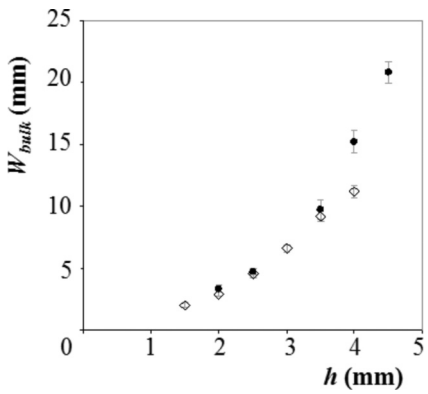

FIG. 7. Dependency of the mixing length W_{bulk} on the local solution depth h. ◊ and • show W_{bulk} for the concave and convex meniscus, respectively. W_{bulk} were measured at both reactor lateral walls and at $y = 1/2L_y$. Error bars shows standard deviation obtained for six independent experiments.

first hundred seconds, front development is identical for both experimental conditions. The still expanding fronts were arc shaped. Later the fronts started to adopt the asymptotic shape with respect to the geometry of the solution, which was given by the geometry of the reactor and shape of the meniscus. Under the concave meniscus condition, the leading edge kept a shape with positive curvature for $t < 250$ s. Approximately at $t = 250$ s, a V shape with negative curvature began to develop. Depth of that V shape grew in time. On the other hand, the leading edge held a shape with positive curvature during the entire experiment under the convex meniscus condition.

Under both experimental conditions and in given time, the rightmost and the leftmost positions of the leading edge delineate the mixing length (W_{surface}) of the liquid motion occurring at the surface. Figure 9 illustrates the procedure of the mixing length W_{surface} evaluation. Under a deformed interface condition, W_{surface} was calculated from the following equation:

$$W_{\text{surface}} = \sqrt{(h_{\max} - h_{\min})^2 + (x_{\text{LEmax}} - x_{\text{LEmin}})^2}, \qquad (6)$$

where $h_{\max}$ and $h_{\min}$ are the maximal and the minimal height of the liquid layer, respectively. x_{LEmax} and x_{LEmin} are the rightmost and the leftmost position of the leading edge, respectively.

Figures 8(c) and 8(d) depicts development of W_{surface} for concave and convex meniscus conditions, respectively. The plots correspond to the experiments shown in Figs. 8(a) and 8(b). For both experimental conditions, development of the mixing length W_{surface} can be divided into three periods. Under a concave meniscus condition, W_{surface} increased up to a maximum during the first period. The increase was followed by a drop to a minimum during the second period. During the third period, W_{surface} was again increasing. Although such a scenario was seen for experiments performed under the concave meniscus condition, the absolute values varied from experiment to experiment. Under the convex meniscus condition, development of W_{surface} looks very similar to the concave meniscus condition during the first two periods. Again, an increase is followed by a decrease. However, different development was seen under convex meniscus condition during the third period. A very slow decrease of W_{surface}, as seen in Fig. 8(d), or nearly constant W_{surface} was observed.

Finally, Fig. 10 shows dependency of front velocities on liquid layer depth h. The front velocities were evaluated from the space-time plots as a slope of the trace of the leading edge. For all experiments, the space-time plots were constructed at three positions y_i; $y_1 = 1/2\ L_y$, $y_2 = 1$ mm, and $y_3 = 14$ mm. At y_i, maximal value of solution depth ($h_{\max}$) or minimal value of solution depth ($h_{\min}$) were reached. Under both experimental conditions, the velocity is increasing with the solution depth. For the concave meniscus condition, the increase is nearly linear, and standard deviations are relatively small. For the convex meniscus condition, different behavior was observed. First, the velocity values are usually higher than those obtained for the concave meniscus condition. Second, for particular L_z, nearly identical velocities measured at $h_{\max}$ and $h_{\min}$ were obtained. However, the velocity increase was observed, but it was related to L_z. Third, the standard deviations are bigger than those obtained for concave meniscus condition.

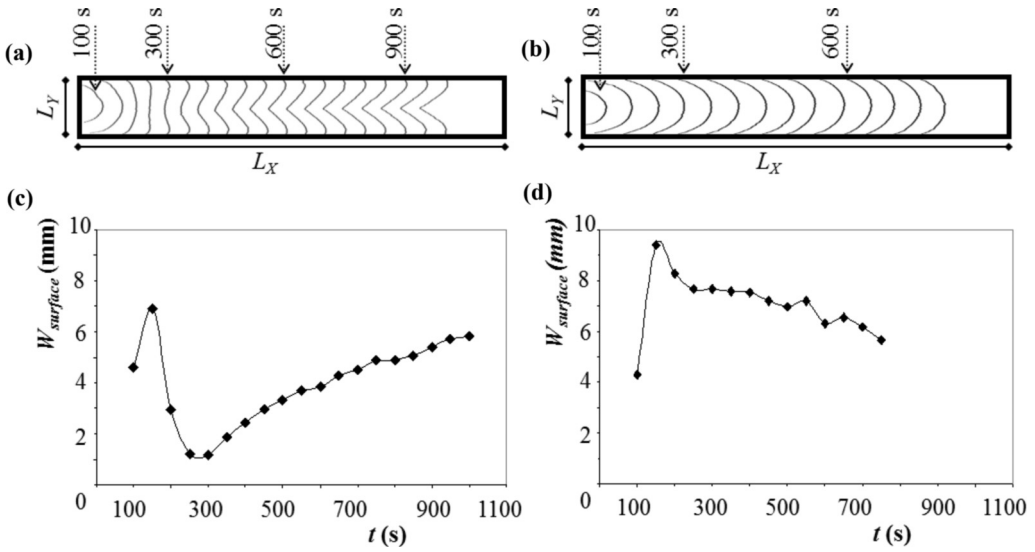

FIG. 8. Development of the front leading edge and the corresponding mixing length $W_{surface}$. (a), (c) The concave meniscus; (b), (d) the convex meniscus.

IV. DISCUSSION

Development of IAA reaction fronts was studied in a liquid system, where natural convection can be induced. The surface tension measurements had shown that the reaction mixture does not contain any surface active component. Since temperature of the solutions was kept constant, there is no driving force at the interface which could lead to onset of Marangoni convection. Therefore, the buoyancy force remains as the only source of convection in the studied IAA reaction system.

In order to guarantee the same initial conditions, the fronts were always initiated chemically as circular waves. The chemical initiation has several advantages in comparison to the electrochemical one. First, the exact location and the exact time of the front initiation is under full control. Second, the wave is initiated at the liquid-gas interface, from where it invaded the reaction solution. On the other hand, when electrochemical method would be used, both exact time and exact location of the front would not be predictable. Since the electrodes have to be immersed into the reaction solution, the initiation place will be somewhere on the electrode surface, but not necessarily at the liquid-gas interface. Due to the buoyancy effect, such a front will first travel towards the interface, and then it will invade the rest of the reaction solution. Moreover, the electric current has to be applied on the system in duration longer than 2 min in order to initiate the chemical front. However, the exact time is unpredictable. Therefore, the priority was given to the chemical initiation.

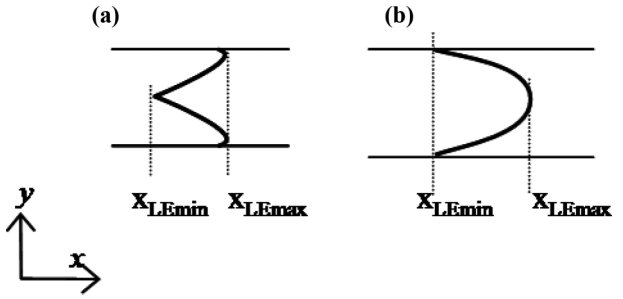

FIG. 9. Determination of the mixing length $W_{surface}$. (a) The concave meniscus and (b) the convex meniscus.

The influence of buoyancy driven convection on development of the IAA reaction fronts propagating through the horizontal layer of the reaction solution was already studied. The buoyancy-driven convection controls both the front velocity and the front shape. Although the front velocity is constant in time [3,7,17,22], it is increasing with the solution depth [7,20,22]. Several authors have reported about tilted fronts seen in lateral views [3,7,17,20,22,23]. For top views, V-shaped fronts were seen in the shallow layer of the reaction solution, while parabolic fronts were seen in the reaction solution deeper than 13 mm.

Our results are in very good agreement with the literature [3,7,20]. Our results and the previous studies [7] coincide with each other in the experiments performed with the solution

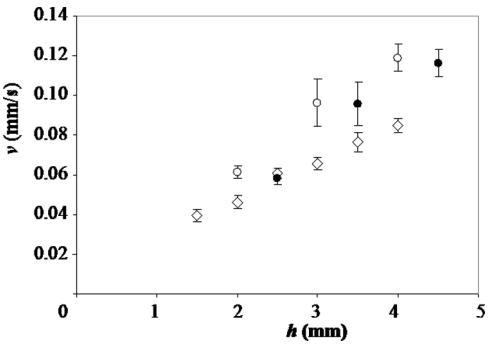

FIG. 10. Dependence of the front velocity on the local liquid layer depth h. ◊ show velocity, which was obtained for concave meniscus experiment and evaluated at both positions: at $1/2\ L_y$ and at reactor side walls. For the convex meniscus condition, • represent velocity measured at $y = 1/2\ L_y$, and ○ represents velocity measured at both reactor walls. Error bars show standard deviation obtained for six independent experiments.

TABLE II. Front velocities observed for liquid layer depth $h = 4$ mm.

Concave meniscus	0.085 ± 0.004 mm/s
Convex meniscus	0.118 ± 0.007 mm/s
Šebestíková *et al.* [7]	0.11 ± 0.01 mm/s

depth $h = 4$ mm. The front velocities, which are shown in Table II, are very similar. Dependency of the velocities on h and dependence of mixing lengths of the tilted fronts on h are also in accord with previous studies [3,7,20]. However, some differences between experiments performed with the concave and convex meniscus were observed.

The interface deformation influences the front velocity, front shape, mixing length W_{surface}, and mixing length W_{bulk}.

The front velocities and mixing length W_{bulk} became sensitive to the interface deformation when the solution depth h was higher than 2.5 mm. For $h < 2.5$ mm, the velocities and the mixing length W_{bulk} were independent on the shape of the meniscus. This behavior can be understood as a boundary effect of the reactor bottom on the buoyancy flow. For $h > 2.5$ mm, the velocity values and W_{bulk} values were observed to be higher in experiments performed with the convex meniscus. The relation between the observed differences and the shape of the meniscus is discussed below.

Development of the front shape can be divided into three consequent periods.

During the first period, development of the circular fronts was not affected by the boundary of the system. The borders of the system were still far enough that their presence did not influence the buoyancy-driven flow. The circular fronts were expanding in all directions under both experimental conditions. The fronts grew faster at the liquid-gas interface. Curvature of the fronts was positive. During this period, increase of mixing length W_{surface} was observed under both experimental conditions. In the used channel reactors, the first period ended when the fronts reached the lateral walls. At this moment, the mixing length W_{surface} was at its maximum. During the first period, the front shape was developing like the shape of fronts, which would be propagating in a system with an ideally flat surface.

During the second period, the fronts are adapting to the shape of the liquid layer. The fronts were not expanding anymore towards the reactor lateral walls, but they started to move along them. The front shape was also adapting to the new condition, which is expressed in the decreasing mixing length W_{surface}. Under the convex meniscus condition, the changes were not so dramatic like under the concave meniscus condition. Under the convex meniscus condition, the front curvature slightly decreased, but it was higher than zero. At the end of the second period, fronts propagating under the convex meniscus condition reached the asymptotic shape. On the other hand, under the concave meniscus condition, the curvature was decreasing, and it became nearly zero at the end of the second period. As a consequence of the wall boundary effect on the flow, the fronts were always a bit curved at the lateral walls, which means that the minimal value of W_{surface} cannot be zero. However, curvature of the front part, which was far enough from the lateral walls, was zero at this time. The minimal value of W_{surface} signalized the end of the second period for both experimental conditions.

During the third period, asymptotic behavior of the front was seen. Under the convex meniscus condition, the fronts had a shape with positive curvature. The mixing length W_{surface} was nearly constant. On the other hand, the V-shaped front was seen under the concave meniscus condition. The front curvature became negative. The mixing length and depth of the cusp were increasing.

The shape of any chemical wave (the pulse or the front) is connected to the mass flow across the wave. In pure reaction-diffusion (RD) media, the wave development is controlled by diffusion flux across the wave. Since the intensity of the diffusion flux is constant along the wave, the wave holds shape with positive curvature. When the wave is growing, the curvature is asymptotically decreasing toward zero. The asymptotic shape of the RD waves is a planar wave. However, Brazhnik *et al.* [24] reported that a single wave having a asymptotic shape with negative curvature can also exist, when the following condition is fulfilled: mass flow of some reaction species dominates in some particular direction. Recently, formation of the V shape was observed in the chlorite-tetrathionate reaction system, as a result of the buoyancy-driven flow [10]. However, this V shape was the shape of the wave end, while the leading edge was parabolic. Stability of the observed V shape depended on solution depth. For a deep solution layer, the depth of the V shape was constant. Contrary to that, for shallow layers, oscillation of the depth of the V shape was reported [10].

In our experiments, both diffusion and the buoyancy flow contribute to the mass flow across the front. However, the buoyancy flow dominates. For a 2D arrangement of the reaction-diffusion-convection system, numerical simulation [20,23] predicted one roll traveling together with the wave. Those simulations show that the lighter products are rising behind the front since the heavier reactants are sinking ahead of the front. For a 3D arrangement of our experiments, a sketch of possible flow maps is shown in Fig. 11. Under both conditions, the light products move from the reactor bottom up to the liquid surface. Since the surface is not flat but is deformed, the surface flow is formed. The surface flow pushes the light products to the highest point of the surface. Therefore, under the concave meniscus condition, the ascending flow has to split into two streams at the lowest part of the surface located at $1/2\ L_y$. Those streams then continue moving up to the highest point of the surface, which is located at the reactor lateral

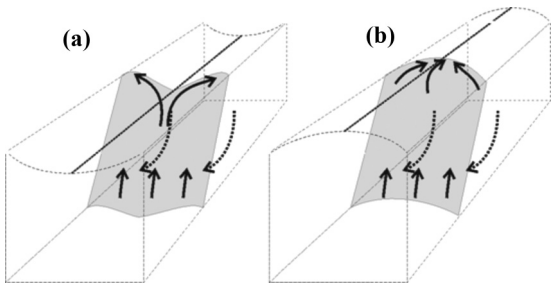

FIG. 11. The flow maps. (a) The concave meniscus; (b) the convex meniscus. Solid-line arrows show direction of the flow behind the front. Dotted-line arrows depict the flow ahead of the front.

walls. Since the mass flow across the front is controlled by the buoyancy flow, which pushes the chemical species in one particular direction, the formation of the asymptotic V-shaped fronts and lower velocity values achieved by those fronts are results of the stream splitting. Under the convex meniscus condition, stream splitting does not occur. The highest part of the surface is at the middle of the reactor at $1/2\ L_y$, and the buoyancy flow pushes the chemical species from bulk and from both lateral walls towards the center. Therefore, those waves were faster under convex meniscus condition. In the case of an ideal flat surface, no surface flow will be generated. The shape of the front would depend only on the bulk flow geometry.

V. CONCLUSIONS

For the buoyantly unstable reaction solution, the shape of the liquid-gas interface significantly influences front development. The fronts were under the effect of the nonuniform distribution of the solution depth. The local solution depth depended on the meniscus shape. The same signs of curvature of the deformed interface and the asymptotic shape of the fronts were observed. Under the concave meniscus condition, both the deformed interface and the asymptotic V shape of the fronts had negative curvature. On the other hand, under the convex meniscus condition, both the deformed interface and the fronts had positive curvature. Due to the differences in flow distribution, fronts propagating under the concave meniscus condition were a bit slower than those propagating under the convex meniscus condition. However, the front velocities were increasing with the liquid layer depth, which is in very good agreement with previous experimental and numerical studies [7,20].

ACKNOWLEDGMENTS

The author acknowledges Dr. P. Basařová (Institute of Chemical Technology, Prague, Czech Republic) and Dr. M. Zedníková (Institute of Chemical Process Fundamentals of the ASCR, Czech Republic), who provided surface tension measurements. The author also acknowledges Dr. J. Ježek (Institute of Organic Chemistry and Biochemistry of the ASCR, Czech Republic) for language corrections. The presented results were obtained due to support afforded by (1) the Czech Science Foundation GACR through Grant No. P105/10/0919 and (2) Institutional Research Plan No. AV0Z20600510.

[1] T. A. Gribschaw, K. Showalter, D. Banville, and I. R. Epstein, J. Phys. Chem. **85**, 2152 (1981).
[2] A. Hanna, A. Saul, and K. Showalter, J. Am. Chem. Soc. **104**, 3838 (1982).
[3] J. A. Pojman and I. R. Epstein, J. Phys. Chem. **94**, 4966 (1990).
[4] M. Böckmann and S. Müller, Phys. Rev. E **70**, 046302 (2004).
[5] L. Forštová, H. Ševčíková, M. Marek, and J. H. Merkin, J. Phys. Chem. A **104**, 9136 (2000).
[6] L. Rongy, G. Schuszter, Z. Sinko, T. Toth, D. Horvath, A. Toth, and A. De Wit, Chaos **19**, 023110 (2009).
[7] L. Šebestíková and M. J. B. Hauser, Phys. Rev. E **85**, 036303 (2012).
[8] M. A. Budroni, L. Rongy, and A. De Wit, Phys. Chem. Chem. Phys. **14**, 14619 (2012).
[9] F. Rossi, M. A. Budroni, N. Marchettini, and J. Carballido-Landeira, Chaos **22**, 037109 (2012).
[10] E. Pópity-Tóth, D. Horváth, and A. Tóth, Chaos **22**, 037105 (2012).
[11] L. Rongy, P. Assemat, and A. De Wit, Chaos **22**, 037106 (2012).
[12] S. C. Müller, T. Plesser, and B. Hess, Ber. Bunsen-Ges. Phys. Chem. **89**, 654 (1985).
[13] K. Matthienssen and S. Müller, Phys. Rev. E **52**, 492 (1995).
[14] K. Matthienssen, H. Wilke, and S. Müller, Phys. Rev. E **53**, 6056 (1996).
[15] M. Diewald, K. Matthienssen, S. C. Müller, and H. R. Brand, Phys. Rev. Lett. **77**, 4466 (1996).
[16] H. Miike, H. Yamamoto, S. Kai, and S. Müller, Phys. Rev. E **48**, R1627 (1993).
[17] J. A. Pojman, I. R. Epstein, T. J. McManus, and K. Showalter, J. Phys. Chem. **95**, 1299 (1991).
[18] D. Vasquez, J. Littley, J. W. Wilder, and B. F. Edwards, Phys. Rev. E **50**, 280 (1994).
[19] L. Šebestíková, J. D'Hernoncourt, M. J. B. Hauser, S. Müller, and A. De Wit, Phys. Rev. E **75**, 026309 (2007).
[20] L. Rongy, N. Goyal, E. Meiburg, and A. De Wit, J. Chem. Phys. **127**, 114710 (2007).
[21] N. Jarrige, I. B. Malham, J. Martin, N. Rakotomalala, D. Salin, and L. Talon, Phys. Rev. E **81**, 066311 (2010).
[22] E. Pópity-Tóth, D. Horváth, and A. Tóth, J. Chem. Phys. **135**, 074506 (2011).
[23] B. F. Edwards, J. W. Wilder, and K. Showalter, Phys. Rev. A **43**, 749 (1991).
[24] P. K. Brazhnik and V. A. Davydov, Phys. Lett. A **199**, 40 (1995).